Shock Waves Manuscript-Nr.
(will be inserted by hand later)

Calculation of stagnation streamline quantities in hypersonic blunt body flows

Arno Klomfass and Siegfried Müller

[1] Ernst-Mach-Institut, Eckerstr. 4, 79104 Freiburg
[2] Institut für Geometrie und Praktische Mathematik, Templergraben 55, 52056 Aachen

Received

Abstract. An approximate method for the efficient calculation of stagnation-streamline quantities in hypersonic flows about spheres or cylinders is suggested. Based on the local similarity of the flow field the two-dimensional Navier-Stokes equations are simplified to a one-dimensional approximation for the stagnation streamline. These equations are solved with an implicit finite-volume scheme. Comparisons with fully two–dimensional Euler and Navier–Stokes calculations for flows about spheres are presented, that include perfect gas flows and flows in chemical non-equilibrium. Comparisons with a number of experiments conclude this report.

Key words: Non-equilibrium, Stagnation Streamline, Local Similarity, Navier-Stokes equations, Chemically reacting flows

Nomenclature

a_f	frozen speed of sound [m/s]
γ_f	ratio of frozen specific heats [-]
ρ_α	partial density of component α [kg/m^3]
v	velocity vector [m/s]
$\underset{\sim}{j}_\alpha$	diffusion flux vector [kg/m^2 s]
$\underset{\sim}{q}$	molecular heat flux vector [W/m^2]
ω_α	chemical production rate [kg/m^3 s]
$\underset{\approx}{\tau}$	shear stress tensor [N/m^2]
p	hydrostatic pressure [N/m^2]
E	total energy [J/kg]
H	total enthalpy [J/kg]
e_α	specific energy of component α [J/kg]
h_α	specific enthalpy of component α [J/kg]
T	temperature [K]
x_α	mass fraction of component α [-]
y_α	mole fraction of component α [-]
D	diffusion coefficient $[kg/m^3 s]$
μ	viscosity coefficient $[kg/ms]$
λ	heat-conduction coefficient $[W/mK]$

Correspondence to: klomfass@emi.fhg.de

1 Introduction

The hypersonic flow about a spacecraft entering the atmosphere at orbital velocity is characterized by two main features: the high kinetic energy of the flow that leads to strong molecular collisions, and the low density of the atmosphere that results in small molecular collision rates. Molecular collisions with sufficient energy lead to the excitation of higher molecular modes and to changes in the gas composition as molecules dissociate. Due to small collision rates local non-equilibrium may be relevant. This is the case if the respective equilibration times of the chemical composition and the molecular energy distribution are comparable to the mean resident time of the gas in the flow field. In the following only local chemical non-equilibrium is taken into account, i.e. local thermal equilibrium is assumed.

The non-equilibrium flow is then described mathematically by the conservation equations for the mass, the momentum and the total energy of the gas mixture and additional balance equations for the partial densities of the components. The physical model enters these equations via the expressions for the chemical production rates and the molecular fluxes.

The calculation of stagnation-streamline quantities in hypersonic flows about spheres and cylinders requires the solution of the governing equations with two independent spatial variables. The computational domain has to be extended at least beyond the boundaries of the subsonic region of the shock layer, cf. Fig. 1. The computation is thus rather time consuming and not suitable for parametric studies or a fast analysis of a specific flow situation.

In the approach suggested in the present work the governing equations are simplified by reducing the number of independent spatial variables. This leads to a quasi one-dimensional approximation for the stagnation streamline in the considered flows. The simplified set of equations, in the following called dimensionally reduced Navier-Stokes equations (DRNSE), can be solved numerically within some minutes on a standard workstation or PC, even with very high spatial resolution. This makes the approach useful e.g. for evaluating the effects of

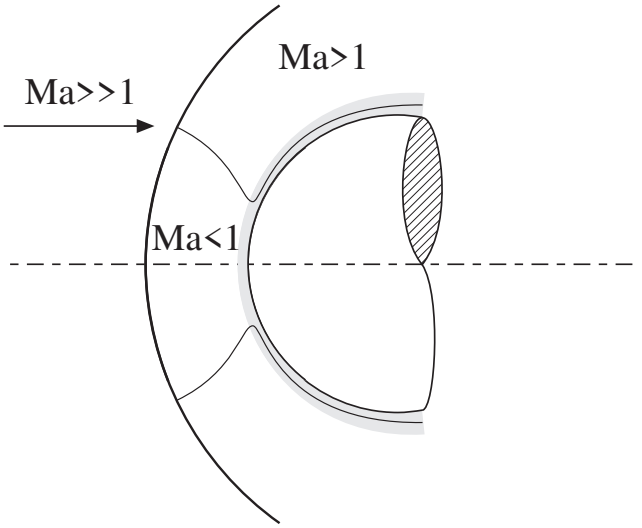

Fig. 1. Hypersonic blunt body flow

finite-rate chemistry on the convective stagnation-point heating of re-entry vehicles or planetary probes. The application is however limited to simple flows about spheres or cylinders. The DRNSE are based on the local similarity of the stagnation-streamline area in the considered flow fields. This local similarity has already been studied by several scientists, cf. Kao (1964), Probstein and Hayes (1966), Conti (1966), Vinokur (1970). Numerical integration of equations, similar to those investigated here, has been attempted by Johnston and Hendricks (1978) with however limited success.

The aim of this work is to provide a numerical tool for pre- and post-experimental analysis, examination of thermochemical models and the fast and reliable determination of stagnation-point heat fluxes. Within the present paper the DRNSE are validated against two-dimensional calculations for flows about spheres, where exactly the same physical model has been used. Furthermore, comparisons with the formula of Fay and Riddell for the stagnation-point heat flux and comparisons with experiments are presented.

2 Fluid dynamic balance equations

The volumetric balance equations for the masses of the chemical components, the momentum and the total energy of the gas mixture are

$$\frac{\partial\,\rho_\alpha}{\partial\,t} + \operatorname{div}(\rho_\alpha \underset{\sim}{v}) + \operatorname{div}(\underset{\sim}{j}_\alpha) = \omega_\alpha\,, \tag{1}$$

$$\frac{\partial\,\rho\underset{\sim}{v}}{\partial\,t} + \operatorname{div}(\rho\underset{\sim}{v}\circ\underset{\sim}{v} + p\underset{\approx}{E}) + \operatorname{div}(\underset{\approx}{\tau}) = \underset{\sim}{0}\,, \tag{2}$$

$$\frac{\partial\,\rho E}{\partial\,t} + \operatorname{div}(\rho H \underset{\sim}{v}) + \operatorname{div}(\underset{\approx}{\tau}\underset{\sim}{v}) + \operatorname{div}(\underset{\sim}{q}) = 0\,, \tag{3}$$

where the density, the total specific energy and the total specific enthalpy are given by

$$\rho = \sum_\alpha \rho_\alpha\,, \quad E = e + \underset{\sim}{v}^2/2, \quad H = E + p/\rho. \tag{4}$$

The balance equations (1) can be added up to obtain the mass conservation equation. As the sum of the diffusion fluxes and the sum of the species mass production vanish by definition, there is

$$\frac{\partial\,\rho}{\partial\,t} + \operatorname{div}(\rho\underset{\sim}{v}) = 0. \tag{5}$$

If the gas composition is assumed constant or in local equilibrium, the set of balance equations (1) can be replaced by (5).

Relations for the molecular fluxes, i.e. the diffusion fluxes, the stress tensor and the total heat flux are obtained from a Chapman–Enskog expansion of the Boltzmann equation, cf. Hirschfelder et al. (1965),

$$\underset{\sim}{j}_\alpha = -D_\alpha\,\operatorname{grad} x_\alpha\,, \tag{6}$$

$$\underset{\approx}{\tau} = -\mu\left\{\operatorname{grad}\underset{\sim}{v} + (\operatorname{grad}\underset{\sim}{v})^T - \frac{2}{3}(\operatorname{div}\underset{\sim}{v})\underset{\approx}{E}\right\}\,, \tag{7}$$

$$\underset{\sim}{q} = -\lambda\,\operatorname{grad} T + \sum_\alpha h_\alpha \underset{\sim}{j}_\alpha\,. \tag{8}$$

Here bulk viscosity, pressure- and thermo-diffusion have been neglected. The relations are then essentially identical with the empirical approaches of Fick, Newton, and Fourier. Together with the balance equations (1) - (3) they form the Navier–Stokes equations for the non-equilibrium flow of a mixture of thermally perfect gases.

The purely algebraic relations for the pressure, the energies, and the transport coefficients are provided by constitutive relations given in Sec. 5.

It has to be noted, that the Navier–Stokes equations do not apply for flows with severe deviations from equilibrium. They fail to provide correct solutions for the structure of strong shock waves. The application is in practice limited to flows, where the thickness of the shock wave is small compared to the thickness of the shock layer.

The balance equations (1) - (3) and the molecular fluxes (6) - (8) are obtained in specific coordinates when the respective contravariant basis vectors are introduced into the definitions of the gradient and the divergence operators,

$$\operatorname{grad}\varphi = \sum_{\lambda=1}^{3}\frac{\partial\,\varphi}{\partial\,x^\lambda}\circ\underset{\sim}{g}^\lambda, \quad \operatorname{div}\varphi = \sum_{\lambda=1}^{3}\frac{\partial\,\varphi}{\partial\,x^\lambda}\cdot\underset{\sim}{g}^\lambda,$$

where $\varphi = \varphi(t, \underset{\sim}{x})$ may be either a scalar, a vector or a tensor. In the next section spherical coordinates are considered. The major part of the formulas given there is quoted from Bird et al. (1960).

3 Derivation of the DRNSE

To derive the DRNSE the original equations are first cast in spherical coordinates for the rotationally symmetric flow problem. A separation of variables technique is then applied to a suitable set of flow quantities. These flow quantities are represented as products of unknown

functions of the radial coordinate and empirically prescribed functions of the angular coordinate. The differentiation with respect to the angular coordinate can then be carried out to obtain the DRNSE. The success of this approach of course depends on the chosen sets of flow quantities and prescribed functions of the angular coordinate. Details will be given in Sec. 3.2.

3.1 Spherical coordinates

The arrangement of the spherical coordinates (r, θ, ϕ) is illustrated in Fig. 2.

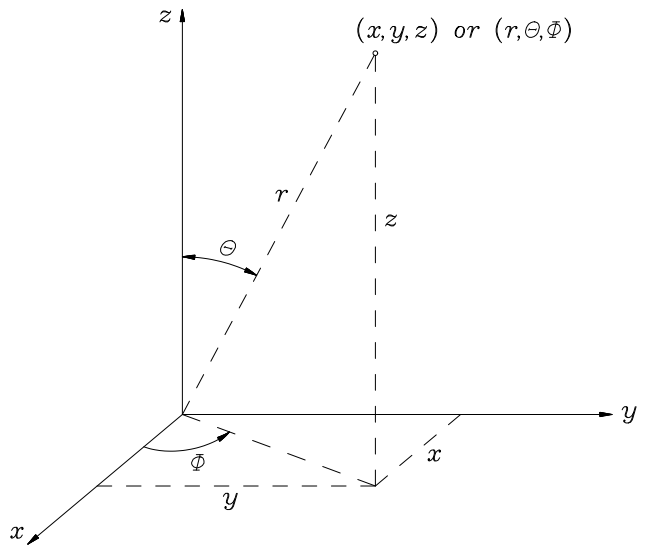

Fig. 2. Spherical coordinates

Since we are dealing with rotationally symmetric problems, we can directly take into account, that $\partial/\partial\phi = 0$ and $v_\phi = 0$ if the direction of the undisturbed flow is the z-axis ($\theta = 0$) in Fig. 2. The application of the divergence operator to a scalar p, a vector $\underset{\sim}{v}$ and a tensor $\underset{\approx}{\tau}$ then leads to the following relations, cf. Bird et al. (1960), pp. 739C - 739D,

$$\mathrm{div}\,(\underset{\approx}{E}p)\,|_r = p_{,r}\,, \tag{9}$$

$$\mathrm{div}\,(\underset{\approx}{E}p)\,|_\theta = \frac{1}{r}p_{,\theta}\,, \tag{10}$$

$$\mathrm{div}\,(\underset{\sim}{v}) = v_{r,r} + \frac{2}{r}v_r + \frac{\cot\theta}{r}v_\theta + \frac{1}{r}v_{\theta,\theta}\,, \tag{11}$$

$$\mathrm{div}\,(\underset{\approx}{\tau})\,|_r = \tau_{rr,r} + \frac{2}{r}\tau_{rr} + \frac{\cot\theta}{r}\tau_{r\theta} + \frac{1}{r}\tau_{r\theta,\theta} - \frac{1}{r}\tau_{\theta\theta} - \frac{1}{r}\tau_{\phi\phi}\,, \tag{12}$$

$$\mathrm{div}\,(\underset{\approx}{\tau})\,|_\theta = \tau_{r\theta,r} + \frac{3}{r}\tau_{r\theta} + \frac{\cot\theta}{r}\tau_{\theta\theta} + \frac{1}{r}\tau_{\theta\theta,\theta} - \frac{\cot\theta}{r}\tau_{\phi\phi}\,. \tag{13}$$

The symbols $|_r$ and $|_\theta$ denote the $r-$ and $\theta-$components of the respective vectors. The above relations can directly be introduced into the original balance equations. The vector $\underset{\sim}{v}$ in (11) can also be identified with $\rho\underset{\sim}{v}$, $\underset{\approx}{\tau}\underset{\sim}{v}$, $\underset{\sim}{q}$ to obtain the required expressions for these quantities. In the same manner the above relation for the tensor $\underset{\approx}{\tau}$ can be applied to $\rho\underset{\sim}{v}\circ\underset{\sim}{v}$ to get

$$\mathrm{div}\,(\rho\underset{\sim}{v}\circ\underset{\sim}{v})\,|_r = (\rho v_r v_r)_{,r} + \frac{2}{r}(\rho v_r v_r) + \frac{\cot\theta}{r}(\rho v_r v_\theta) + \frac{1}{r}(\rho v_r v_\theta)_{,\theta} - \frac{1}{r}(\rho v_\theta v_\theta)\,, \tag{14}$$

$$\mathrm{div}\,(\rho\underset{\sim}{v}\circ\underset{\sim}{v})\,|_\theta = (\rho v_r v_\theta)_{,r} + \frac{3}{r}(\rho v_r v_\theta) + \frac{\cot\theta}{r}(\rho v_\theta v_\theta) + \frac{1}{r}(\rho v_\theta v_\theta)_{,\theta}\,. \tag{15}$$

The following elements of the stress tensor were taken from Bird et al. (1960), pp. 90.

$$\tau_{rr} = -\mu\left\{\frac{4}{3}v_{r,r} - \frac{4}{3}\frac{v_r}{r} - \frac{2}{3}\frac{\cot\theta}{r}v_\theta - \frac{2}{3}\frac{v_{\theta,\theta}}{r}\right\}\,, \tag{16}$$

$$\tau_{r\theta} = -\mu\left\{-\frac{1}{r}v_\theta + v_{\theta,r} + \frac{1}{r}v_{r,\theta}\right\}\,, \tag{17}$$

$$\tau_{\theta\theta} = -\mu\left\{-\frac{2}{3}v_{r,r} + \frac{2}{3}\frac{v_r}{r} + \frac{4}{3}\frac{v_{\theta,\theta}}{r} - \frac{2}{3}\frac{\cot\theta}{r}v_\theta\right\}\,, \tag{18}$$

$$\tau_{\phi\phi} = -\mu\left\{-\frac{2}{3}v_{r,r} + \frac{2}{3}\frac{v_r}{r} + \frac{4}{3}\frac{\cot\theta}{r}v_\theta - \frac{2}{3}\frac{v_{\theta,\theta}}{r}\right\}\,. \tag{19}$$

3.2 Approximations used within the DRNSE

In deriving the DRNSE we assume, that a suitable set of flow quantities $\mathbf{f}$ can be expressed, at least approximately, by a separation of variables technique, i.e.

$$\mathbf{f}(r,\theta) = \mathbf{f}^*(\theta)\,\bar{\mathbf{f}}(r). \tag{20}$$

As is discussed in Klomfass and Müller (1996), this approach can also be looked at as a special case of an asymptotic expansion.

In our approach we prescribe the functional dependencies $\mathbf{f}^*(\theta)$ on the basis of intuitive arguments. To derive a physically meaningful approximation several constraints for the possible choices for $\mathbf{f}^*(\theta)$ have to be considered. These constraints arise from geometrical-, symmetry- and boundary-conditions.

The symmetry of the flow field implies that the quantities v_r, p, T, x_α are symmetric to the axis $\theta = 0$. In contrast, the angular velocity component v_θ behaves anti-symmetric. The undisturbed parallel supersonic free-stream is a boundary condition that should be satisfied. If an isothermal, fully catalytic wall is considered, constant surface temperature and mass fractions impose further conditions. In a first approximation it may be assumed, that these quantities are functions of the radial coordinate alone. With regard to the pressure the Newtonian theory provides the approximation

$$p_w - p_\infty = \rho_\infty v_\infty^2 \cos^2\theta \qquad (21)$$

for the surface pressure in the hypersonic limit, i.e. when $Ma \to \infty$, cf. Anderson (1989). This is a useful approximation even at finite Mach numbers $Ma \gg 1$, provided the bow shock is about concentric to the sphere or cylinder surface, respectively. In view of these constraints, the following relations seem promising:

$$\begin{aligned} v_r &= \overline{v}_r(r)\cos\theta\,, \\ v_\theta &= \overline{v}_\theta(r)\sin\theta\,, \\ p &= p_\infty + \overline{p}(r)\cos^2\theta\,, \\ T &= \overline{T}(r)\,, \\ x_\alpha &= \overline{x}_\alpha(r)\,. \end{aligned}$$

It should be noted, that the relations for the temperature and the mass fractions are less favorable if an adiabatic or non-catalytic wall is considered, respectively. Furthermore, the approximation fails to provide a correct description for the temperature behind the shock, which of course depends on the shock angle. This may however be tolerated as the main interest focuses on the boundary layer part of the flow field. In terms of the chosen relations, the boundary conditions are

Free-stream:	Stagnation-point:
$\overline{p} = 0$	$\overline{p}_{,r} = 0$
$\overline{v}_r = u_\infty$	$\overline{v}_r = 0$
$\overline{T} = T_\infty$	$\overline{T} = T_W$ or $\overline{T}_{,r} = 0$
$\overline{v}_\theta = u_\infty$	$\overline{v}_\theta = 0$ or $\overline{v}_{\theta,r} = 0$
$\overline{x}_\alpha = x_{\alpha,\infty}$	$\overline{x}_\alpha = x_{\alpha,W}$ or $\overline{x}_{\alpha,r} = 0$

These boundary conditions describe the supersonic parallel free stream, a no-slip or slip wall, an isothermal or adiabatic wall, and a fully catalytic or a non-catalytic wall.

The above relations are substituted into the balance equations in spherical coordinates. In the resulting expressions for $\rho \underset{\sim}{v} \circ \underset{\sim}{v}$ terms with coefficients $\sin\theta$, or higher powers of $\sin\theta$ can be neglected, as they are small against the remaining terms, as $\theta \to 0$. In the equation for the angular momentum the factor $\sin\theta$ can be factorized, thus leaving an equation for $\overline{v}_\theta$.

In a final step the equations are now specified for the stagnation streamline by letting $\theta \to 0$. This limiting process renders the DRNSE which can be written formally as

$$\overline{\mathbf{u}}_{,t} + \overline{\mathbf{F}}^I_{,r} + \overline{\mathbf{F}}^V_{,r} + (\overline{\mathbf{G}}^I + \overline{\mathbf{G}}^V)\, r^{-1} = \mathbf{S},$$

$$\overline{\mathbf{u}} = \begin{pmatrix} \rho_1 \\ \vdots \\ \rho_N \\ \rho\overline{v}_r \\ \rho\overline{v}_\theta \\ \rho E \end{pmatrix}, \overline{\mathbf{F}}^I = \begin{pmatrix} \rho_1\overline{v}_r \\ \vdots \\ \rho_N\overline{v}_r \\ \rho\overline{v}_r^2 + p \\ \rho\overline{v}_r\overline{v}_\theta \\ \rho\overline{v}_r H \end{pmatrix}, \overline{\mathbf{F}}^V = \begin{pmatrix} j_{r1} \\ \vdots \\ j_{rN} \\ \overline{\tau}_{rr} \\ \overline{\tau}_{r\theta} \\ q_r + \overline{\tau}_{rr}\overline{v}_r \end{pmatrix},$$

$$\overline{\mathbf{G}}^I = \begin{pmatrix} 2\,\rho_1(\overline{v}_r + \overline{v}_\theta) \\ \vdots \\ 2\,\rho_N(\overline{v}_r + \overline{v}_\theta) \\ 2\,\rho\overline{v}_r(\overline{v}_r + \overline{v}_\theta) \\ 3\,\rho\overline{v}_\theta(\overline{v}_r + \overline{v}_\theta) - 2\,\overline{p} \\ 2\,\rho H(\overline{v}_r + \overline{v}_\theta) \end{pmatrix},$$

$$\overline{\mathbf{G}}^V = \begin{pmatrix} 2\,j_{r1} \\ \vdots \\ 2\,j_{rN} \\ 2\,(\overline{\tau}_{rr} - \overline{\tau}_{\theta\theta} + \overline{\tau}_{r\theta}) \\ -\overline{\tau}_{\theta\theta} + 3\,\overline{\tau}_{r\theta} \\ 2(q_r + \overline{\tau}_{rr}\overline{v}_r + \overline{\tau}_{r\theta}\overline{v}_r + \overline{\tau}_{\theta\theta}\overline{v}_\theta) \end{pmatrix}.$$

It should be noted, that both the inviscid and viscous metric terms $\overline{\mathbf{G}}^I$, $\overline{\mathbf{G}}^V$ consist of two contributions. One arises from the introduction of the spherical coordinates in the balance equations and another from the evaluation of the derivatives with respect to θ in the context of the DRNSE approximation. The source terms in the DRNSE are unaltered against the original expressions.

More details are given in Klomfass and Müller (1996). There, also the DRNSE for flows about cylinders are presented, which are derived analogously.

4 The numerical method

An implicit time integration method is applied to obtain steady-state solutions of the DRNSE, which are approximated by the finite-volume equations

$$\frac{\overline{\mathbf{u}}_i^{n+1} - \overline{\mathbf{u}}_i^n}{\Delta t} + \frac{\overline{\mathbf{F}}_{i+1/2}^{n+1} - \overline{\mathbf{F}}_{i-1/2}^{n+1}}{\Delta r} + \overline{\mathbf{G}}_i^{n+1} = \mathbf{S}_i^{n+1}\,, \qquad (22)$$

with $\Delta t = t^{n+1} - t^n$ and $\Delta r = (r_{i+1} - r_{i-1})/2$. In the above notation, both the viscous and inviscid contributions to the fluxes and metric terms are included in $\overline{\mathbf{F}}$ and $\overline{\mathbf{G}}$.

The viscous fluxes at the cell interfaces $i \pm 1/2$ and at the cell centers i are approximated by second order accurate finite differences as functions of the respective values at points $i-1, i$ and $i+1$. The inviscid fluxes at the cell interfaces are approximated by the averages of the inviscid fluxes at points $i-1, i$ and $i, i+1$, respectively. The finite-volume approximation is thus second order accurate in space and exactly identical to a centered finite-difference approximation.

The unknowns $\overline{\mathbf{u}}^{n+1}$, $\overline{\mathbf{F}}^{n+1}$, $\overline{\mathbf{G}}^{n+1}$ and $\mathbf{S}^{n+1}$ at time $t^{n+1} = t^n + \Delta t$ are extrapolated from their values at time t^n by means of a truncated taylor expansion. For $\mathbf{q}$ being any of the above quantities there is

$$\mathbf{q}^{n+1} = \mathbf{q}^n + \left.\frac{\partial\,\mathbf{q}}{\partial\,\mathbf{w}}\right|^n \Delta\mathbf{w}^n\,,\ \Delta\mathbf{w}^n = \mathbf{w}^{n+1} - \mathbf{w}^n\,. \qquad (23)$$

At this stage we introduce the primitive variables $\mathbf{w}$,

$$\mathbf{w} = \left(\overline{v}_r, \overline{v}_\theta, \overline{T}, \overline{p}, \overline{x}_\alpha\right)^T,$$

as dependent variables. This is not strictly necessary, it however simplifies the incorporation of the boundary

conditions and the derivation of the jacobians $\partial\mathbf{q}/\partial\mathbf{w}$ considerably. Introducing (23) into (22) and rearranging terms renders

$$\mathbf{a}_i\Delta\mathbf{w}^n_{i-1} + \mathbf{b}_i\Delta\mathbf{w}^n_i + \mathbf{c}_i\Delta\mathbf{w}^n_{i+1} = - \left(\overline{\mathbf{F}}^n_{i+1/2} - \overline{\mathbf{F}}^n_{i-1/2} + \Delta r\overline{\mathbf{G}}^n_i - \Delta r\mathbf{S}^n_i\right) , \quad (24)$$

$$\mathbf{c}_i = \frac{\partial\,\overline{\mathbf{F}}^n_{i+1/2}}{\partial\,\mathbf{w}_{i+1}} - \frac{\partial\,\overline{\mathbf{F}}^n_{i-1/2}}{\partial\,\mathbf{w}_{i+1}} + \frac{\partial\,\overline{\mathbf{G}}^n_i}{\partial\,\mathbf{w}_{i+1}}\Delta r ,$$

$$\mathbf{a}_i = \frac{\partial\,\overline{\mathbf{F}}^n_{i+1/2}}{\partial\,\mathbf{w}_{i-1}} - \frac{\partial\,\overline{\mathbf{F}}^n_{i-1/2}}{\partial\,\mathbf{w}_{i-1}} + \frac{\partial\,\overline{\mathbf{G}}^n_i}{\partial\,\mathbf{w}_{i-1}}\Delta r ,$$

$$\mathbf{b}_i = \frac{\partial\,\overline{\mathbf{F}}^n_{i+1/2}}{\partial\,\mathbf{w}_i} - \frac{\partial\,\overline{\mathbf{F}}^n_{i-1/2}}{\partial\,\mathbf{w}_i} + \frac{\partial\,\overline{\mathbf{G}}^n_i}{\partial\,\mathbf{w}_i}\Delta r - \frac{\partial\,\mathbf{S}^n_i}{\partial\,\mathbf{w}_i}\Delta r + \frac{\partial\,\overline{\mathbf{u}}^n_i}{\partial\,\mathbf{w}_i}\frac{\Delta r}{\Delta t} .$$

The whole set of equations for the interior points $i = 2,\ldots,N-1$ of the computational domain can be written in matrix notation as

$$\mathbf{A}^n\Delta\mathbf{w}^n = \mathbf{RHS}^n , \quad (25)$$

where $\mathbf{A}$ is a square block-tridiagonal matrix. In this notation the products $\mathbf{a}_2\Delta\mathbf{w}^n_1$ and $\mathbf{c}_{N-1}\Delta\mathbf{w}^n_N$ that contain the boundary values $\mathbf{w}_1$ and $\mathbf{w}_N$ are included on the right hand side. Dirichlet boundary conditions are incorporated by assigning the desired value to the respective variables w_1 or w_N and setting the corresponding Δw_1 or Δw_N to zero. Neuman boundary conditions, which are relevant for the stagnation-point ($i = 1$), are approximated by finite differences and expressed in terms of Δw^n, i.e.

$$w^{n+1}_{1,r} = 0 = \frac{4}{3}\Delta w^n_2 - \frac{1}{3}\Delta w^n_3 - \Delta w^n_1 + \frac{4}{3}w^n_2 - \frac{1}{3}w^n_3 - w^n_1 . \quad (26)$$

This relation is added to equation (25) to eliminate the unknown Δw^n_1. Note, that the above relation holds for an equidistant grid only.

Steady-state solutions are obtained asymptotically by successive evaluations of (25). The iteration scheme is formally identical with a Newton-Raphson iteration that makes the right hand side zero, which corresponds here to the conservative steady-state flow equations. Due to the implicit formulation timesteps with large Courant numbers can be realized and a few hundred steps are usually sufficient to obtain a practically converged solution. The computation is initialized with $\mathbf{w}_i, i = 1, N$ interpolated linearly between free-stream and appropriately guessed stagnation-point conditions.

In each time step, the block-tridiagonal system of equations (25) has to be solved for $\Delta\mathbf{w}^n$. A Gaussian elemination with pivoting is used for this task. In the elemination, the block-tridiagonal structure is taken into account to efficiently reduce computation time.

A computation is usually started with about 100 equally spaced grid points. The number of points is successively doubled upon convergence of the stagnation-point heat-flux.

The described finite-volume approximation is appropriate for low Reynolds-number flows, where the molecular fluxes are significant and thick shock waves exist. Solutions with thin shock waves cannot be obtained with this method, due to the central approximation of the inviscid fluxes. For these cases a shock-fitting strategy is used.

4.1 Shock-fitting procedure

If shock-fitting is applied, the computational domain contains only the shock-layer part of the stagnation streamline. As the steady-state shock position is a priori unknown, it is calculated simultaneously with the shock-layer flow. For given data at t^n the shock position at t^{n+1} is determined from the shock speed. The computational grid is then fitted to the new shock position and the finite-volume equations are evaluated with the post-shock conditions at t^{n+1} as upstream boundary conditions ($i = N$). As the changes in shock position per timestep are negligible compared to the shock layer thickness, the same balance equations for stationary control volumes are used.

The shock speed and the post-shock conditions are determined from the Rankine-Hugoniot relations (RHR), an additional compatibility relation (CR) and the constituitive relations. For a chemically frozen gas the RHR are

$$\left[v_t\right] = 0 , \quad (27)$$

$$\left[\rho(v_n - V_s)\right] = 0 , \quad (28)$$

$$\left[\rho(v_n - V_s)^2 + p\right] = 0 , \quad (29)$$

$$\left[h + \frac{1}{2}(v_n - V_s)^2\right] = 0 , \quad (30)$$

$$\left[x_\alpha\right] = 0 . \quad (31)$$

The shock-normal and -tangential basis vectors $\underset{\sim}{g}_n$ and $\underset{\sim}{g}_t$ define the velocity components

$$v_t = \underset{\sim}{v}\,\underset{\sim}{g}_t \quad , \quad v_n = \underset{\sim}{v}\,\underset{\sim}{g}_n , \quad V_s = \underset{\sim}{v}_s\,\underset{\sim}{g}_n \quad , \quad (32)$$

where $\underset{\sim}{V}_s$ denotes the shock speed. The flow velocities v_n and v_t are here identical with v_r and v_θ as the shock front is normal to the stagnation streamline.

The post-shock conditions can be calculated from the RHR if shock speed and upstream flow conditions are given. The shock speed itself has to be iterated until the post-shock conditions satisfy the discretized compatibility relation $\mathcal{F} = 0$,

$$\mathcal{F} = \Delta^S_B p - \left[a_f\rho\right]^S_B \Delta^S_B v_r + \left[a^2_f\rho\frac{v_{\theta,\theta}}{r}\right]^S_B \delta t + \Phi^C_B \quad (33)$$

The CR has been derived from the two-dimensional, unsteady Euler equations, cf. Klomfass (1995). It describes the propagation of a sound wave along the left-running characteristic $\overline{BS}$ that intersects the shock at $t^n + \delta t$, as is illustrated in Fig. 3.

In (33) the Δ-operator denotes the difference between indicated points and the brackets denote the average between indicated points, e.g. $\Delta^S_B p = p_S - p_B$, $[\rho]^S_B =$

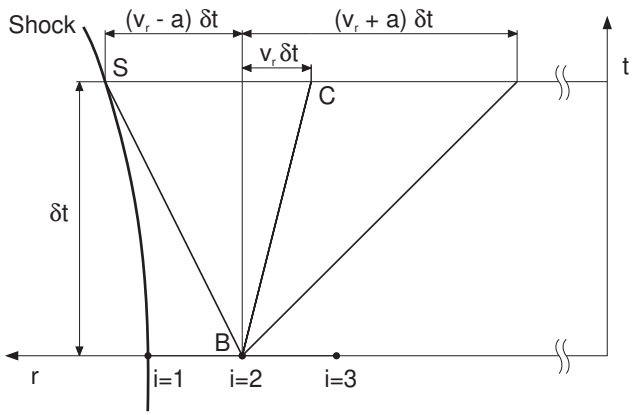

Fig. 3. Shock-fitting

$(\rho_B + \rho_S)/2$. Given the shock position r_S in $t^n + \delta t$, the positions of points B and C follow from

$$r_B = r_S - \left[v_r - a_f\right]_B^S \delta t\,, \qquad r_C = r_B + \left[v_r\right]_B^C \delta t\,. \quad (34)$$

In the DRNSE approximation the shock is assumed concentric to the spherical or cylindrical body and the cross-derivative in (33) is thus given as $v_{\theta,\theta} = \overline{v}_\theta$. The relaxation term Φ in (33) is defined as

$$\Phi = \left[(\gamma_f - 1)\rho\right] \sum_\alpha \left[e_\alpha - \frac{R_\alpha T}{\gamma_f - 1}\right] \Delta x_\alpha\,. \quad (35)$$

The relaxation term is evaluated between the points B and C, i.e. along the material pathline. As the conditions in point C at $t^n + \delta t$ are unknown at the time of calculation, the values from the corresponding point at time t^n are used as an approximation. This approach provides second order accuracy in the steady-state solution.

The iteration of the shock speed that renders $\mathcal{F} = 0$ is here achieved with the method of bisection. Within this iteration a local time step δt is applied, as indicated above. This time step is chosen as to make point B identical with the grid point $i = 2$ next to the shock. Once the shock speed is determined the shock position is updated with the global time step Δt.

Shock slip is not taken into account here, i.e. the molecular fluxes are not included in RHR and CR. This approximation is sufficiently accurate for high to moderate Reynolds-number flows, where the molecular fluxes immediately behind the shock are negligible compared to the macroscopic fluxes.

5 Constitutive relations

We consider air as a mixture of the five components N_2, O_2, NO, N and O, which are assumed to be thermally perfect gases. The pressure is thus given by

$$p = \sum_\alpha p_\alpha = \sum_\alpha \frac{2}{3}\rho_\alpha e_\alpha^{(tr)} = \sum_\alpha \rho_\alpha R_\alpha T\,. \quad (36)$$

The internal energy of a component is assumed to consist of independent translational, electronic, rotational and vibrational contributions and a reference energy $e_\alpha^{(0)}$ to account for energy changes in chemical reactions, i.e.

$$e_\alpha = e_\alpha^{(tr)} + e_\alpha^{(el)} + e_\alpha^{(rot)} + e_\alpha^{(vib)} - e_\alpha^{(0)} \quad . \quad (37)$$

The values of $e_\alpha^{(0)}$ are choosen such, that the energies of N and O vanish at zero Kelvin. For N_2, O_2 and NO the values of $e_\alpha^{(0)}$ are thus the corresponding dissociation energies.

The rotational and vibrational contributions are described by the models of rigid rotation and truncated harmonic oscillation, cf. Clarke and McChesney (1964), pp. 80. These contributions vanish for atomic components. Equations of state $e_\alpha(T)$ are obtained from partition functions, cf. Clarke and McChesney (1964). These are based on the assumption of local thermal equilibrium, i.e. the existence of Boltzmann distributions with a common temperature T for all modes.

The chemical production rates ω_α are calculated from rate equations,

$$\omega_\alpha = M_\alpha \sum_r \left(\nu_\alpha^{(r'')} - \nu_\alpha^{(r')}\right) \times \left\{ k^{(r')} \prod_\beta (c_\beta)^{\nu_\beta^{(r')}} - k^{(r'')} \prod_\beta (c_\beta)^{\nu_\beta^{(r'')}} \right\}\,, \quad (38)$$

where $\nu_\alpha^{(r')}$ and $\nu_\alpha^{(r'')}$ denote the stoichometric coefficients that define the reactions r.

The rate constants $k^{(r')}$ of the endothermic reactions are calculated according to the Arrhenius-type correlations of Park (1985) and the rate constants of the exothermic reactions are deduced from the principle of detailed balance, i.e.

$$k^{(r'')} = \quad k^{(r')}(T) \,/\, K_r(T)\,, \quad (39)$$

where the equilibrium constants K_r are given in terms of the partition functions of the species associated with the respective reaction, cf. Clarke and McChesney (1964). In Klomfass (1995) more details about the thermochemical model and extensions to thermal non-equilibrium are given.

The viscosity μ of the gas mixture is approximated by the viscosities μ_α of the pure species and the mixing rule of Herning and Zipperer,

$$\mu = \sum_{\alpha=1}^{N} \frac{\mu_\alpha y_\alpha}{\phi_\alpha} \quad , \quad \phi_\alpha = \sum_\beta y_\beta \sqrt{M_\beta / M_\alpha}\,, \quad (40)$$

where y denotes mole fractions and M molar masses, cf. Zipperer and Herning (1936). The viscosities of the pure species are calculated from the curve fits of Metz, which are based on experimental and theoretical data, cf. Metz (1995).

Finally, the heat conduction and diffusion coefficients are approximated by assumed constant Prandtl and Schmidt numbers,

$$\lambda = \frac{c_p\,\mu}{Pr} \quad , \quad D_\alpha = D = \frac{\mu}{\rho Sc}\,, \quad (41)$$

where values of 0.7 have been used for either number Pr and Sc. A further discussion of the molecular-flux model is found in Klomfass et al. (1993).

Table 1. Test cases 1.1 - 1.20: Results

			DRNSE		Euler/Fay&Riddell		rel.deviation	
#	Ma	Re	q [kW/m^2]	δ/R_{sph}	q [kW/m^2]	δ/R_{sph}	Δ q /q	$\Delta\delta/\delta$
1.1	2	1.E3	2.775	0.2615	2.719	0.3383	0.0206	-0.21
1.2	5	1.E3	32.34	0.1357	32.13	0.1559	0.0065	-0.13
1.3	10	1.E3	213.3	0.1115	189.5	0.1350	0.1260	-0.17
1.4	20	1.E3	1316	0.1008	1141	0.1299	0.1530	-0.22
1.5	50	1.E3	16380	0.0917	12560	0.1284	0.3040	-0.28
1.6	2	1.E4	8.458	0.2565	8.599	0.3383	-0.0164	-0.24
1.7	5	1.E4	95.4	0.1387	101.1	0.1559	-0.0602	-0.11
1.8	10	1.E4	592.4	0.1208	599.3	0.1350	-0.0115	-0.10
1.9	20	1.E4	3687	0.1148	3608	0.1299	0.0219	-0.11
1.10	50	1.E4	40330	0.1101	39710	0.1284	0.0156	-0.14
1.11	2	1.E5	26.17	0.2547	27.19	0.3383	-0.0375	-0.24
1.12	5	1.E5	295.4	0.1391	321.3	0.1559	-0.0806	-0.11
1.13	10	1.E5	1848	0.1227	1895	0.1350	-0.0248	-0.09
1.14	20	1.E5	11430	0.1182	11410	0.1299	-0.0018	-0.09
1.15	50	1.E5	120000	0.1161	125600	0.1284	-0.0446	-0.09
1.16	2	1.E6	83.5	0.2546	85.99	0.3383	0.0289	-0.24
1.17	5	1.E6	936.3	0.1392	1016	0.1559	-0.0748	-0.11
1.18	10	1.E6	6004	0.1232	5993	0.1350	0.0018	-0.09
1.19	20	1.E6	36460	0.1190	36080	0.1299	0.0105	-0.08
1.20	50	1.E6	37130	0.1177	397100	0.1284	-0.0650	-0.08

6 Results and Discussion

In the following we will again focus on flows about spheres. To assess the accuracy of the DRNSE three sets of test cases are considered. The first two sets cover generic flows of a perfect gas and some generic high-enthalpy flows in chemical nonequilibrium. The third set contains a number of high-enthalpy flows, for which experimental results are available.

The accuracy of the DRNSE is assessed by comparisons with two-dimensional Euler and Navier-Stokes calculations on the basis of two issues: the shock standoff-distance and the stagnation-point heat-flux.

In the test cases 1.1 to 1.20 a perfect gas is considered, with $R = 289$ J/kgK, $\gamma = 1.4$, viscosity according to Sutherland's law, cf. Anderson (1989), and a constant Prandtl number of 0.7. The sphere radius is 0.1 m and the wall temperature is 300 K. Viscous flows ranging from Mach number 2 to 50 with Reynolds numbers of 1000 to 1.0×10^6 have been calculated with the DRNSE-method for perfect gas. It has to be noted that these test cases are more or less without physical relevance due to the perfect gas model. They serve as purely numerical tests.

Two-dimensional inviscid reference-solutions are obtained from the Euler-scheme, a detailed description of which is given in Klomfass (1995). Reference values for the stagnation-point heat-fluxes have been determined with the formula of Fay and Riddell (1958), which for $Pr = Sc$ or $Le = 1$ respectively may be written for any gas model as

$$q_w = 0.76\,(Pr)^{-0.6}\ \ (\rho_e \mu_e)^{0.4} (\rho_w \mu_w)^{0.1} \times (H_e - H_w)\,\sqrt{(\partial\, v/\partial\, y)_e} \qquad (42)$$

with the stagnation-point velocity gradient $(\partial v/\partial y)_e$. Subscript e denotes the value of a quantity at the outer edge of the boundary layer.

The conditions at the outer edge of the boundary layer, which are required in this formula, have been identified with the adiabatic stagnation-point conditions predicted by the Euler-calculations. The data used in Fay & Riddell's formula for test cases 1.1 - 1.20 and 2.1 - 2.6 can be found in Klomfass and Müller (1996).

For the perfect gas there is no question concerning the thermochemical equilibration of the boundary layer. Fay and Riddell's formula can thus be employed without further assumptions.

Computational results for test cases 1.1 to 1.20 are summarized in Tab. 1. There are only five different Euler calculations, which render the shock-standoff distances in the inviscid flows. In all test cases, the free-stream temperature was 300 K. The Mach and Reynolds numbers have been tuned via the free-stream values of velocity and density. Reynolds numbers in Tab. 1 are based on the sphere diameter. As the Stanton number,

$$St = \frac{q}{\rho_\infty V_\infty (H_\infty - H_w)} \quad , \qquad (43)$$

is a dimension-free quantity it depends on Mach and Reynolds number only if γ and Pr are considered fixed. From dimensional analysis it can be seen that the Stanton number is proportional to $1/\sqrt{Re}$. Thus the stagnation-point heat-fluxes are proportional to $\sqrt{Re}$ in test cases 1.1 to 1.20.

The following conclusions can be derived from the computed results. First, the shock standoff-distance is always underestimated by the DRNSE. The deviation increases with decreasing Mach number or increasing shock standoff-distance. This behaviour may be attributed to the assumption of a newtonian-like pressure distribution, which holds respectively for high Mach numbers or small shock standoff-distances only. Second, the stagnation-point heat-fluxes deviate to about 8% from the results obtained with the formula of Fay and Riddell. It has to be noted however, that the latter itself is only a correlation to numerical solutions and does not provide exact results. Exceptions to these conclusions are found in test cases 1.3 to 1.5. In these test cases the boundary-layer extents over a significant portion of the shock layer. Fay

Table 2. Free stream conditions 2.1 - 2.6

#	T_w [K]	R_{sph}[m]	V[m/s]	p[Pa]	T[K]	Ma	Re	x_{N_2}	x_{O_2}	x_{NO}	x_N	x_O
2.1	1500	0.1524	7600	4.18	212	26.0	22980	0.7654	0.2345	1E-5	1E-5	1E-5
2.2	1500	0.1524	7600	40.3	264	23.3	151700	0.7654	0.2345	1E-5	1E-5	1E-5
2.3	1500	0.1524	4100	75.9	270	12.4	148460	0.7654	0.2345	1E-5	1E-5	1E-5
2.4	1500	0.1524	4100	276	251	12.9	613800	0.7654	0.2345	1E-5	1E-5	1E-5
2.5	300	0.05	3568	90.2	196	12.7	87280	0.7654	0.2345	1E-5	1E-5	1E-5
2.6	300	0.05	2500	90.2	196	12.7	61160	0.7654	0.2345	1E-5	1E-5	1E-5

Table 3. Test cases 2.1 to 2.6: Results

	DRNSE		DRNSE (Euler b/c)/Fay&Riddell		2D-NS	
#	q [MW/m^2]	δ/R_{sph}	q_{fr} [MW/m^2]	q_{eq} [MW/m^2]	q [MW/m^2]	δ/R_{sph}
2.1	1.093	0.070	0.91	2.06	1.125	0.074
2.2	2.064	0.058	1.45	4.67	2.349	0.060
2.3	0.526	0.081	0.49	0.86	0.675	0.087
2.4	1.079	0.076	0.85	1.65	1.580	0.081
2.5	1.338	0.092	1.27	1.58	1.343	0.097
2.6	0.493	0.105	0.50	0.50	0.548	0.114

and Riddell's formula is therefore not applicable in the above mentioned way. Note also, that the boundary-layer thickness grows with Mach number.

In the test cases 2.1 to 2.6 five-component air-flows in chemical non-equilibrium have been investigated. The respective free-stream conditions are summarized in Tab. 2.

Given Reynolds numbers are here based on the sphere radius. A non-catalytic wall has been assumed throughout. The DRNSE results are here compared to two-dimensional Navier-Stokes calculations based on a finite-volume scheme (cf. Müller (1993), Müller et al. (1993)), where an identical thermochemical model has been used.

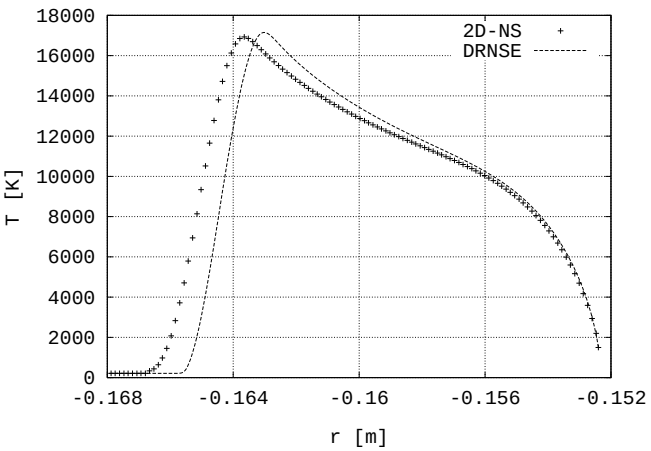

Fig. 4. Case 2.1, Temperature

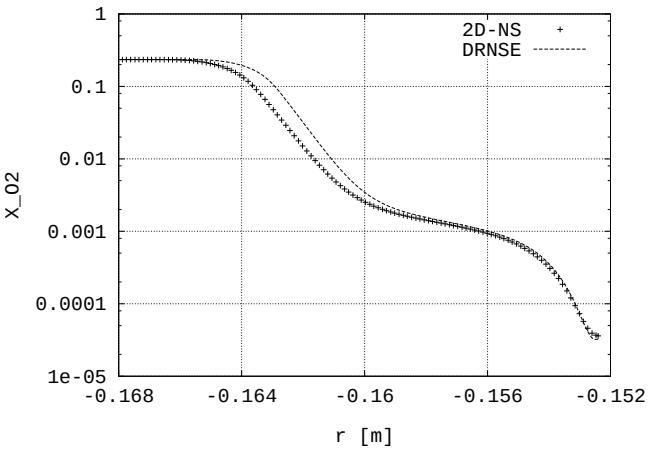

Fig. 6. Case 2.1, Mass Fraction of X_{O_2}

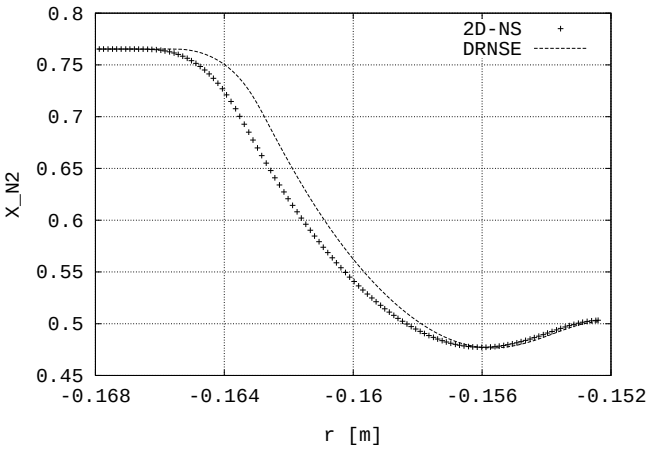

Fig. 5. Case 2.1, Mass Fraction of X_{N_2}

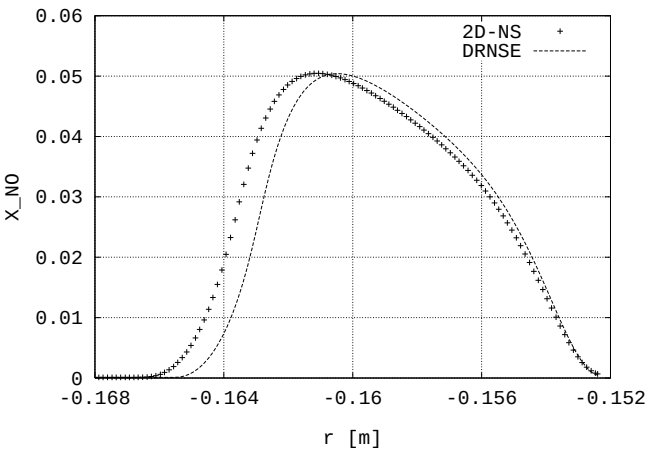

Fig. 7. Case 2.1, Mass Fraction of X_{NO}

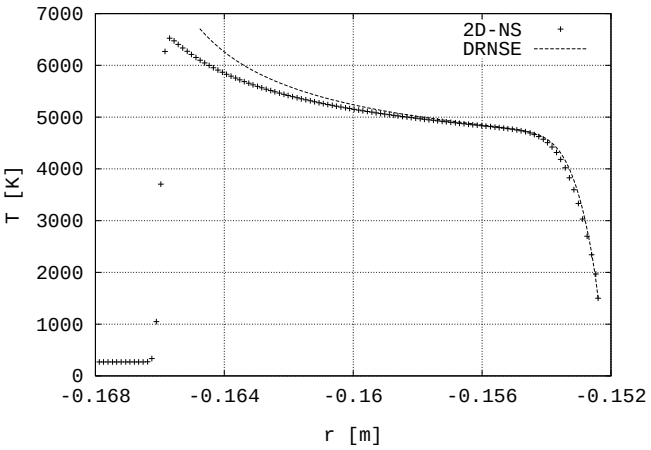

Fig. 8. Case 2.3, Temperature

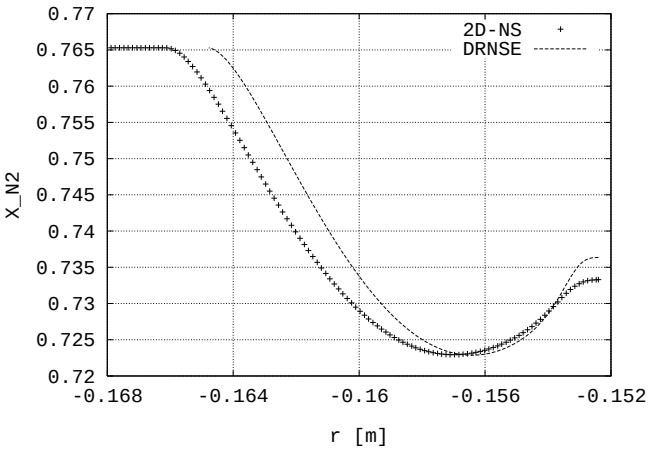

Fig. 9. Case 2.3, Mass Fraction of X_{N_2}

The grid resolution is about 120 × 130 equidistant points in the 2D-calculations and up to about 2000 equidistant points in the converged DRNSE solutions. Typical CPU times are 8 h for the 2D-method and 5 min for the DRNSE-scheme on a SGI workstation (IRIS–Indigo–R8000).

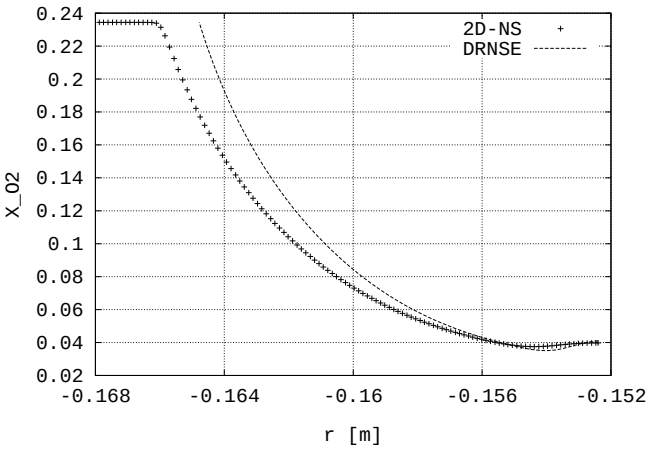

Fig. 10. Case 2.3, Mass Fraction of X_{O_2}

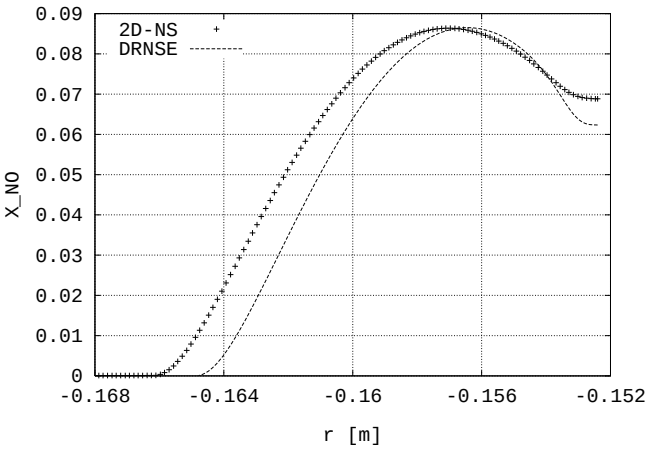

Fig. 11. Case 2.3, Mass Fraction of X_{NO}

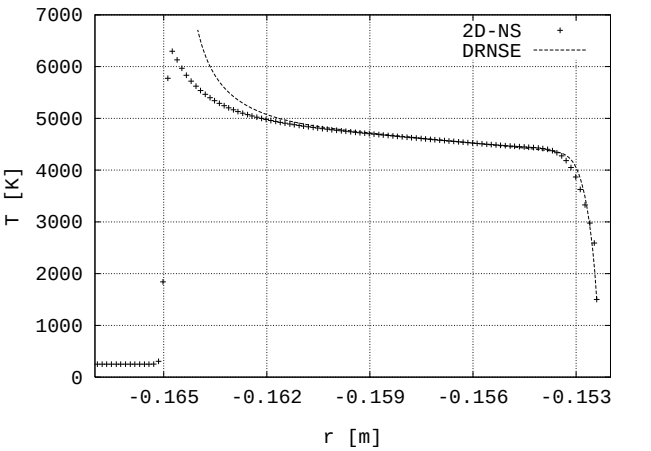

Fig. 12. Case 2.4, Temperature

Results for the temperature and the mass fractions of the molecular species at the stagnation streamline are shown for test case 2.1, 2.3, 2.4 and 2.6 in Figs. 4 - 11. For test case 2.6 no mass fractions are shown, as the flow was found to be chemically frozen.

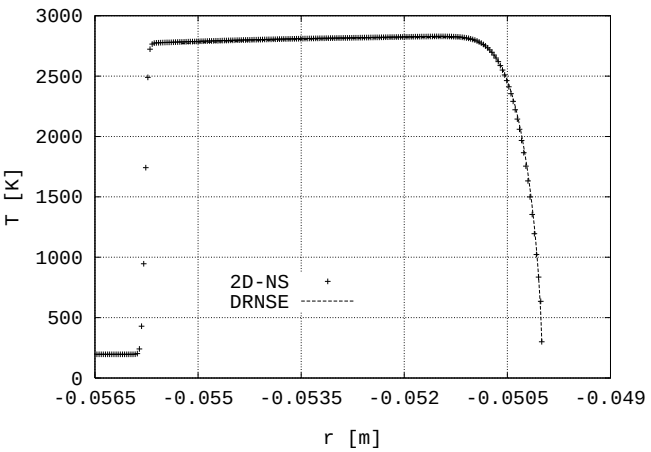

Fig. 13. Case 2.6, Temperature

Table 4. Free stream conditions 3.1 - 3.11

#	T_w	R_{sph}	V	p	T	Ma	Re	x_{N_2}	x_{O_2}	x_{NO}	x_N	x_O
3.1	300	0.0381	3965	12407	1402	5.4	345200	0.7350	0.1730	0.06499	1E-5	0.0270
3.2	300	0.0254	3929	11180	1371	5.4	213400	0.7350	0.1730	0.06499	1E-5	0.0270
3.3	300	0.0254	5301	13090	2359	5.2	119920	0.7410	0.0580	0.03400	1E-5	0.1669
3.4	300	0.0381	5631	13835	2707	5.1	155400	0.7550	0.0230	0.02200	1E-5	0.1999
3.5	300	0.0254	4860	11930	1946	5.4	153400	0.9599	1E-5	1E-5	4E-2	1E-5
3.6	300	0.0381	5144	13530	2200	5.4	223300	0.9599	1E-5	1E-5	4E-2	1E-5
3.7	300	0.0125	2490	3400	345	6.7	217600	0.7654	0.2345	1E-5	1E-5	1E-5
3.8	300	0.0125	3470	9240	853	6.0	175720	0.7654	0.2345	1E-5	1E-5	1E-5
3.9	300	0.0500	3568	90.2	196	12.7	87300	0.7654	0.2345	1E-5	1E-5	1E-5
3.10	300	0.0100	5919	430	790	9.7	11300	0.7490	0.0360	0.03339	1E-5	0.1816
3.11	300	0.0100	4813	470	553	9.9	19990	0.7324	0.1444	0.06899	1E-5	0.0542

Table 5. Test cases 3.1 - 3.11: Results

	DRNSE, non-cat. wall			DRNSE, fully-cat. wall			Experiment
#	q [MW/m^2]	St	H_w [MJ/kg]	q [MW/m^2]	St	H_w [MJ/kg]	q [MW/m^2], ()=St
3.1	13.63	0.0126	-28.442	14.40	0.0125	-29.068	14.11
3.2	15.14	0.0158	-28.370	16.12	0.0156	-29.068	15.26
3.3	34.50	0.0220	-27.345	37.00	0.0216	-28.914	34.51
3.4	32.99	0.0192	-27.381	35.20	0.0189	-29.066	30.26
3.5	27.27	0.0202	-32.243	28.68	0.0197	-33.332	25.00
3.6	26.14	0.0165	-31.967	28.10	0.0163	-33.332	26.31
3.7	4.70	0.0176	-29.065	4.71	0.0176	-29.069	3.70
3.8	14.43	0.0182	-28.539	15.54	0.0180	-29.069	14.00
3.9	1.36	0.0441	-28.210	1.59	0.0445	-29.069	(0.045)
3.10	16.31	0.1137	-22.998	23.64	0.1172	-29.054	21.00
3.11	11.21	0.0823	-26.227	14.40	0.0825	-29.054	15.00

The employed methods provide qualitatively identical results in all test cases. As in the previous set of test cases the tendency of the DRNSE to underpredict the shock standoff-distance is observed. The relative deviations are here however smaller, as the shock standoff-distances are small in comparison with the perfect-gas flows. Note that in case 2.1 the smeared shock could be captured with the DRNSE-scheme, while in the other cases shock-fitting was required. Some notable deviations were observed in the vicinity of the stagnation point in test cases 2.2 to 2.4 which may be attributed to a non-sufficient resolution in the two-dimensional calculations. This becomes apparent in Figs. 9 - 12.

For these test cases large deviations are observed in the calculated stagnation-point heat-fluxes, which are listed in Tab. 3. For cases 2.1, 2.5 and 2.6 the agreement of the heat-fluxes is satisfactory.

As the Fay and Riddell formula covers only the limits of frozen and equilibrium boundary layers, it provides only estimates for the lower and upper limits of the stagnation-point heat-fluxes, which are also listed in Tab. 3. The adiabatic stagnation-point conditions required for the evaluation of (42) have been determined from the DRNSE with Euler boundary-conditions.

In the third set of test cases, Tab. 4, comparisons are made with experimentally determined heat fluxes. Heat fluxes and free-stream conditions for test cases 3.1 to 3.6 have been provided by Wen and Hornung (1995). Note that 3.5 and 3.6 are pure nitrogen flows. Traces of other components have been added for numerical reasons only. Test cases 3.7 to 3.9 have been examined at the TH2 shock-tube at Aachen by several investigators, Vetter (1993), Olivier (1995). Finally 3.10 and 3.11 are results from recent calibration-runs at the HEG facility at DLR Göttingen, Eitelberg and Krek (1995). Fixed surface temperatures of 300 K have been assumed for all test cases. The DRNSE-scheme has here been used to calculate the stagnation-point heat-fluxes for the non-catalytic and the fully-catalytic surface. Results are summarized in Tab. 5.

For test cases 3.1 to 3.9 the DRNSE-results for the stagnation-point heat-fluxes are about the same for catalytic and non-catalytic surfaces. This indicates that the flow fields are close to local equilibrium. The experimental data match with the majority of the DRNSE-results very well (cf. Tab. 5).

It can be observed that the calculated stagnation-point heat-fluxes for the non-catalytic surface are somewhat closer to the experimentally measured values. A larger deviation is found in case 3.7. The flow in this test case is chemically almost frozen and is thus comparable to the flows in test cases 1.12 and 1.13, where the DRNSE performed well against the reference-solutions. The discrepancy observed here can not be explained yet.

The flow fields resulting from test conditions 3.10 and 3.11 are dominated by non-equilibrium effects, as is indicated by the large differences between the non-catalytic and fully catalytic cases. Large differences are also observed in the corresponding stagnation enthalpies H_w, which solely result from different stagnation-point gas-compositions. Negative values for H_w are a consequence of the used convention for the zero Kelvin energies in (37).

It is interesting to note that the Stanton number is hardly influenced by the catalycity of the surface. Nevertheless, the knowledge of the Stanton number alone does not render the wall heat-flux, since the stagnation-point gas-composition — and hence the stagnation enthalpy — is not known a-priori in a non-equilibrium flow. The Stanton number has thus limited value in the anal-

ysis of non-equilibrium flows. In the cases 3.10 and 3.11 the DRNSE-results indicate a high catalycity of the surfaces, although the material used in the experiments is not supposed to show such a tendency. Most probably the assumed reaction rate constants are inappropriate. Larger reaction rates will result in higher heat-fluxes, thus bringing the results for a non-catalytic wall closer to the measured values. It should also be taken into account, that the exact free-stream conditions in the experiments are uncertain to some degree.

7 Conclusions

A useful approximation for the stagnation-streamline quantities in hypersonic blunt-body flows can be obtained from the numerical integration of the dimensionally reduced Navier–Stokes equations. The presented numerical method provides an ideal tool for the investigation of non-equilibrium and near local-equilibrium flows, as it allows a fast, high–resolution calculation of the stagnation-streamline quantities. The method is not limited to airflows but can be easily applied e.g. to other planetary atmospheres by modifying the chemical database. Also models for finite-rate surface-chemistry may be included.

Up to now, only chemical non-equilibrium has been investigated in depth. A first calculation for thermal non-equilibrium is presented in Klomfass et al. (1995) with similar findings.

Investigations for plane two-dimensional flows about cylinders have not been carried out yet. In these flows the shock standoff-distance is larger compared to flows about spheres. It might thus be expected that higher errors in the predictions of the shock standoff-distances and slightly less favorable results for the stagnation-point heat-flux will be found.

Acknowledgement. This work is funded by the Deutsche Forschungsgemeinschaft.

References

Anderson JD (1989) Hypersonic and High Temperature Gas Dynamics. MacGraw-Hill Book Company

Bird RB, Stewart WE, Lightfoot EN (1960) Transport Phenomena. Wiley

Clarke JF, McChesney M (1964) The Dynamics of Real Gases. Butterworths

Conti RJ (1966) A theoretical study of non-equilibrium blunt body flow. J. Fluid Mech. 24(1):65–88

Eitelberg G, Krek RM (1995) privat communication, DLR Göttingen

Fay JA, Riddell FR (1958) Theory of Stagnation Point Heat Transfer in Dissociated Air. J. Aero. Sci. 25(2):73–85

Hirschfelder JO, Curtiss CF, Bird RB (1965) Molecular Theory of Gases and Liquids. Wiley

Johnston KD, Hendricks WL (1978) A Numerical Solution of the Navier-Stokes Equations for Chemically Nonequilibrium, Merged Stagnation Shock Layers on Spheres abnd Two-Dimensional Cylinders in Air, NASA Technical Paper 1227

Kao HC (1964) Hypersonic Viscous Flow Near the Stagnation Streamline of a Blunt Body. AIAA J 2:1892-1897

Klomfass A, Müller S, Ballmann J (1993) Modelling of Transport Phenomenafor the Hypersonic Stagnation Point Heat Transfer Problem. AIAA-Paper 93-5047

Klomfass A (1995) Hyperschallströmungen im thermodynamischen Nichtgleichgewicht. Dissertation RWTH Aachen, Verlag Shaker, Aachen

Klomfass A, Müller S, Ballmann J (1995) Analysis of Non-Equilibrium Hypersonic Blunt Body Flow with the Local Similarity Method. in: Proc. Int. Symposium on Shock Waves, Pasadena, USA

Klomfass A, Müller S (1996) A quasi-onedimensional approach for hypersonic stagnation-point flows. Internal Report No. 121, Institut für Geometrie und Praktische Mathematik, RWTH Aachen

Metz S (1995) Numerische Verfahren zur Berechnung des Stoff- und Impulstransports in Wasserstoff–Luft und Methan–Luft Gemischen. Dissertation RWTH Aachen, Verlag Shaker Aachen

Müller S, Dickopp Ch, Ballmann J, Jeltsch R (1993) Computation of Viscous Hypersonic Nonequilibrium Blunt Body Flow. ZFW 17:125–130

Müller S (1993) Erweiterung von ENO–Verfahren auf zwei Raumdimensionen und Anwendung auf hypersonische Staupunktprobleme. Dissertation, RWTH Aachen, Verlag Shaker, Aachen

Olivier H (1995) privat communication, Stoßwellenlabor RWTH Aachen

Park C (1985) On the Convergence of Computation of Chemically Reacting Flows. AIAA 085-0247

Probstein RF, Hayes WD (1966) Hypersonic Flow Theory. Academic Press, 2nd edition

Vetter M (1993) Hyperschallströmungen von Modellen im Stoßwellenkanal. Dissertation, RWTH Aachen, Verlag Mainz, Wissenschaftsverlag

Vinokur M (1970) On stagnation-point conditions in non-equilibrium inviscid blunt body flows. J. Fluid Mech. 43:49–75

Wen C, Hornung H (1995) Experiments on Hypervelocity Dissociating Flow over Spheres. In: Proc Internat Symposium on Shock Waves, Marseille, France

Zipperer L, Herning F (1936) Beitrag zur Berechnung der Zähigkeit technischer Gasgemische aus den Zähigkeitswerten der Einzelbestandteile. Das Gas- und Wasserfach 4:49

This article was processed by the author using the LaTeX style file *cljour2* from Springer-Verlag.